Eur J Nucl Med Mol Imaging (2009) 36:1483–1494
DOI 10.1007/s00259-009-1123-z

ORIGINAL ARTICLE

^{68}Ga-labeled NOTA-RGD-BBN peptide for dual integrin and GRPR-targeted tumor imaging

Zhaofei Liu · Gang Niu · Fan Wang · Xiaoyuan Chen

Received: 31 December 2008 / Accepted: 10 March 2009 / Published online: 10 April 2009

Abstract
Purpose Radiolabeled Arg-Gly-Asp (RGD) and bombesin (BBN) peptide analogs have been extensively investigated for the imaging of tumor integrin $\alpha_v\beta_3$ and gastrin-releasing peptide receptor (GRPR) expression, respectively. Recently, we designed and synthesized a RGD-BBN heterodimeric peptide from c(RGDyK) and BBN(7–14) through a glutamate linker. The goal of this study was to investigate the dual receptor-targeting property and tumor diagnostic value of RGD-BBN heterodimeric peptide labeled with generator-eluted ^{68}Ga ($t_{1/2}$ 68 min, β^+ 89% and EC 11%), ^{68}Ga-NOTA-RGD-BBN.
Methods RGD-BBN heterodimer was conjugated with 1,4,7-triazacyclononanetriacetic acid (NOTA) and labeled with ^{68}Ga. The dual receptor binding affinity was investigated by a radioligand competition binding assay. The in vitro and in vivo dual receptor targeting of ^{68}Ga-NOTA-RGD-BBN was evaluated and compared with that of ^{68}Ga-NOTA-RGD and ^{68}Ga-NOTA-BBN.
Results NOTA-RGD-BBN had integrin $\alpha_v\beta_3$ and GRPR binding affinities comparable to those of the monomeric RGD and BBN, respectively. The dual receptor targeting property of ^{68}Ga-NOTA-RGD-BBN was validated by blocking studies in a PC-3 tumor model. ^{68}Ga-NOTA-RGD-BBN showed higher tumor uptake than ^{68}Ga-NOTA-RGD and ^{68}Ga-NOTA-BBN. ^{68}Ga-NOTA-RGD-BBN can also image tumors with either integrin or GRPR expression.
Conclusion ^{68}Ga-NOTA-RGD-BBN exhibited dual receptor targeting properties both in vitro and in vivo. The favorable characterizations of ^{68}Ga-NOTA-RGD-BBN such as convenient synthesis, high specific activity, and high tumor uptake, warrant its further investigation for clinical cancer imaging.

Keywords Integrin $\alpha_v\beta_3$ · Gastrin releasing peptide receptor (GRPR) · RGD peptide · Bombesin · Peptide heterodimer · Positron emission tomography (PET) · Gallium-68 (^{68}Ga)

Introduction

Radiolabeled receptor-binding peptides have been extensively investigated over the past decade due to their potential as molecular imaging probes and therapeutic agents [1]. Several peptide-based radiotracers have been developed and have shown promising results in animal studies, and some have been successfully investigated in human clinical trials. Previously, we and others have developed a series of Arg-Gly-Asp (RGD) peptide-based radiotracers for tumor positron emission tomography (PET) and single photon emission computed tomography (SPECT) imaging of integrin $\alpha_V\beta_3$ expression in various animal models [2–5]. Recently, [^{18}F]AH111585 and [^{18}F] galacto-RGD have been under clinical investigation for noninvasive visualization of integrin expression in cancer patients [6–9]. Radiolabeled bombesin (BBN) analogs that specifically target the gastrin-releasing peptide receptor

Electronic supplementary material The online version of this article (doi:10.1007/s00259-009-1123-z) contains supplementary material, which is available to authorized users.

Z. Liu · G. Niu · X. Chen (✉)
The Molecular Imaging Program at Stanford (MIPS),
Department of Radiology and Bio-X Program,
Stanford University School of Medicine,
1201 Welch Rd, P095,
Stanford, CA 94305-5484, USA
e-mail: shawchen@stanford.edu

Z. Liu · F. Wang
Medical Isotopes Research Center, Peking University,
Beijing 100191, China

(GRPR), which is highly expressed in various human cancers of the lung, colon, stomach, pancreas, breast, and prostate [10], have also been investigated for receptor-targeted tumor imaging in both preclinical and clinical studies [11–13].

The monomeric RGD- or BBN-based radiotracers have some limitations, which may hamper their clinical utility for tumor imaging. First, for monomeric peptide-based tumor imaging, the cell-surface targets must be highly expressed in the tumor relative to normal tissues. This may not occur in all tumors during progression of tumor development, invasion, and metastasis. For example, during the dedifferentiation of prostate cancer cells from androgen-controlled to androgen-independent growth, GRPR expression is substantially reduced [14]. Second, the binding affinity of the monomeric peptide for the targeted receptors is relatively low, which may lead to a low tumor uptake and rapid dissociation from the tumor targets [15]. For example, the binding affinity of RGD monomers is about five- to tenfold lower than that of the dimeric RGD peptide analogs [16]. Third, the in vivo pharmacokinetics of the monomeric peptides may be suboptimal. For example, many BBN analogs are excreted via the hepatobiliary route, prohibiting their utility for lower abdomen imaging [17].

Alternatively, we and others have applied the polyvalency effect to develop peptide homomultimers to enhance the affinity and tumor uptake of the peptide tracers [5, 18–21]. We have previously demonstrated that the receptor-binding affinity and tumor uptake of RGD peptides follows the order octamer > tetramer > dimer > monomer [20–23]. Recently, we linked RGD and BBN with a glutamate amino acid residue and synthesized the RGD-BBN heterodimeric peptide which contains motifs recognizing two different receptors (integrin $\alpha_V\beta_3$ and GRPR). The ^{18}F-labeled RGD-BBN heterodimers can bind both integrin and GRPR in vitro and in vivo [22, 24].

In this study, we conjugated the RGD-BBN heterodimer with 1,4,7-triazacyclononanetriacetic acid (NOTA) and labeled the NOTA-RGD-BBN conjugate with ^{68}Ga ($t_{1/2}$ 68 min, β^+ 89% and EC 11%). ^{68}Ga is easily acquired from an in-house ^{68}Ge/^{68}Ga generator (^{68}Ge, $t_{1/2}$ 270.8 days) instead of a medical cyclotron, and allows possible kit formulation for clinical application [25]. The ^{68}Ga-labeled RGD-BBN heterodimer was compared directly to the monomeric RGD and BBN counterparts, and its in vivo dual receptor binding and tumor-targeting properties were also investigated in animal models.

Materials and methods

All commercially obtained chemicals were of analytical grade and used without further purification. ^{125}I-[Tyr^4]BBN (74 TBq/mmol, 2,000 Ci/mmol) was purchased from GE Healthcare (Piscataway, NJ). Na^{125}I was purchased from Perkin-Elmer (Waltham, MA). The peptides aminocaproic acid-BBN(7–14) (Aca-BBN or BBN) and c(RGDyK) (RGD) were synthesized by Peptides International (Louisville, KY). RGD-BBN was synthesized as previously described [24]. *S*-2-(4-Isothiocyanatobenzyl)-1,4,7-triazacyclononane-1,4,7-triacetic acid (*p*-SCN-Bn-NOTA) was purchased from Macrocyclics (Dallas, TX). ^{68}Ga was obtained from a ^{68}Ge/^{68}Ga generator (produced by Cyclotron, Obninsk, Russia) eluted with 4 ml of 0.1 *N* HCl. The semipreparative reversed-phase high-performance liquid chromatography (HPLC) system was the same as that previously reported [3, 4] with a flow rate of 5 ml/min. The mobile phase was changed from 95% solvent A (0.1% trifluoroacetic acid in water) and 5% solvent B (0.1% trifluoroacetic acid in acetonitrile) (0–2 min) to 35% solvent A and 65% solvent B at 32 min. Analytical HPLC has the same gradient system except that a Vydac 218TP54 column (5 μm, 250×4.6 mm) was used and the flow rate was 1 ml/min. The UV absorbance was monitored at 218 nm and the identification of the peptides was confirmed based on the UV spectrum acquired using a PDA detector. The NOTA conjugation and radiolabeling procedures were all performed under metal-free conditions.

NOTA conjugation of peptide

The c(RGDyK) (RGD), Aca-BBN(7–14) (BBN) and RGD-BBN peptides were conjugated with NOTA under standard SCN-amine reaction conditions as we have previously described [3]. Briefly, a solution of 2 μmol of peptide (RGD, BBN, or RGD-BBN) was mixed with 6 μmol of *p*-SCN-Bn-NOTA in sodium bicarbonate buffer (pH 9.0). After stirring at room temperature overnight, the NOTA-conjugated peptides were isolated by semipreparative HPLC. The desired fractions were combined and lyophilized to afford the final product as a white powder. NOTA-c(RGDyK) (NOTA-RGD) was obtained in 61% yield with a 13.4 min retention time on analytical HPLC. Matrix-assisted laser desorption/ionization (MALDI) time-of-flight (TOF) mass spectrometry (MS) was *m/z* 1,070.4 for $[MH]^+$ ($C_{47}H_{68}N_{13}O_{14}S$, calculated molecular weight 1,070.5 Da). NOTA-BBN was obtained in 72% yield with a 22.05 min retention time on analytical HPLC. MALDI-TOF-MS was *m/z* 1504.0 for $[MH]^+$ ($C_{69}H_{102}N_{18}O_{16}S_2$, calculated molecular weight 1503.8). NOTA-RGD-BBN was obtained in 52% yield with a 20.72 min retention time on analytical HPLC. MALDI-TOF-MS was *m/z* 2235.3 for $[MH]^+$ ($C_{102}H_{149}N_{27}O_{26}S_2$, calculated molecular weight 2234.6 Da).

^{68}Ga radiolabeling

The ^{68}Ga labeling was performed according to methods previously described [3]. Briefly, 10 nmol of NOTA-RGD,

NOTA-BBN or NOTA-RGD-BBN peptide was dissolved in 500 μl of 0.1 *M* sodium acetate buffer and incubated with 185 MBq of ^{68}Ga for 10 min at 40°C. ^{68}Ga-NOTA-RGD, ^{68}Ga-NOTA-BBN or ^{68}Ga-NOTA-RGD-BBN was then purified by analytical HPLC and the radioactive peak containing the desired product was collected. After removing the solvent by rotary evaporation, the activity was reconstituted in PBS and passed through a 0.22-μm Millipore filter into a sterile multidose vial for in vitro and in vivo experiments. The labeling was done with a 92% decay-corrected yield for NOTA-RGD (R_t 12.9 min), 95% for NOTA-BBN (R_t 21.8 min), and 90% for NOTA–RGD-BBN (R_t 19.9 min).

Cell lines and animal models

The PC-3 human prostate carcinoma cell line and MDA-MB-435 human melanoma cell line [26, 27] were purchased from the American Type Culture Collection (ATCC, Manassas, VA). PC-3 cells were grown in F-12K nutrient mixture (Kaighn's modification) (Invitrogen, Carlsbad, CA) supplemented with 10% (v/v) fetal bovine serum (FBS, Invitrogen) at 37°C in an atmosphere containing 5% CO_2. MDA-MB-435 cells were grown in L-15 culture medium (Invitrogen) supplemented with 10% (v/v) FBS at 37°C in 100% air. The PC-3 tumor model was generated by subcutaneous injection of 5×10^6 cells into the right front flank of male athymic nude mice (Harlan Laboratories). The MDA-MB-435 tumor model was established by injection of 5×10^6 cells into the right mammary fat pad of female athymic nude mice. The mice were used for microPET studies when the tumor volume reached about 100–300 mm^3 (about 3–4 weeks for PC-3, and about 1–2 weeks for MDA-MB-435). All the animal procedures were performed according to a protocol approved by the Stanford University Institutional Animal Care and Use Committee.

Cell binding assays

In vitro integrin $\alpha_v\beta_3$-binding affinities and specificities of RGD-BBN, NOTA-RGD-BBN, and BBN were compared with those of RGD via displacement cell-binding assays using ^{125}I-c[RGDyK] as the radioligand. ^{125}I-c(RGDyK) was prepared by labeling c(RGDyK) with Na^{125}I at high specific activity (about 44.4 TBq/mmol) according to our previously described method [2]. Experiments were performed on U87MG human glioma cells expressing integrin $\alpha_v\beta_3$ as we have previously described [4, 28]. In vitro GRPR binding affinities and specificities of RGD-BBN, NOTA-RGD-BBN and RGD were compared with those of BBN via displacement cell-binding assays using ^{125}I-[Tyr^4] BBN as the radioligand. Experiments were performed on GRPR-expressing PC-3 cells following our previously described procedure [2, 28]. The best-fit 50% inhibitory concentration (IC_{50}) values were calculated by fitting the data with nonlinear regression using GraphPad Prism (GraphPad Software). Experiments were performed twice with triplicate samples.

Cell uptake and efflux studies

The cell uptake studies were performed as we have previously described with some modifications [2, 28]. Briefly, PC-3 cells were seeded into 12-well plates at a density of 5×10^5 cells per well and incubated (about 18 kBq/well) with ^{68}Ga-labeled tracers at 37°C for 15, 30, 60, and 120 min. Tumor cells were then washed three times with chilled PBS and harvested by trypsinization with 0.25% trypsin/0.02% EDTA (Invitrogen). The cell suspensions were collected and measured in a γ counter (Packard, Meriden, CT). The cell uptake was expressed as the percent added dose (%AD) after decay correction. Experiments were performed twice with triplicate wells. For efflux studies, ^{68}Ga-labeled tracers (about 18 kBq/well) were first incubated with PC-3 cells in 12-well plates for 1 h at 37°C to allow internalization. Then cells were washed twice with PBS, and incubated with cell culture medium for 15, 30, and 60 min. After washing three times with PBS, cells were harvested by trypsinization with 0.25% trypsin/0.02% EDTA. The cell suspensions were collected and measured in a γ counter. Experiments were performed twice with triplicate wells. Data are expressed as percent added dose after decay correction.

MicroPET imaging

PET scans and image analysis were performed using a microPET R4 rodent model scanner (Siemens Medical Solutions) as previously reported [4, 28]. Each PC-3 or MDA-MB-435 tumor-bearing mouse was injected in a tail vein with about 3.7 MBq (100 μCi) of ^{68}Ga-NOTA-RGD, ^{68}Ga-NOTA-BBN or ^{68}Ga-NOTA-RGD-BBN under isoflurane anesthesia (n=4 per group). For static PET, 5-min scans were acquired at 30 min, 1 h, and 2 h after injection. For dynamic PET, 30-min scans (1×30 s, 4×1 min, 1×1.5 min, 4×2 min, 5×3 min; total 15 frames) were started 1 min after injection, and two 5-min static PET images were also acquired at 1 h and 2 h after injection. The images were reconstructed using a two-dimensional ordered-subsets expectation maximum (OSEM) algorithm and no correction was applied for attenuation or scatter. For the blocking experiment, PC-3 tumor-bearing mice were coinjected with c(RGDyK) (RGD) at 10 mg/kg body weight, Aca-BBN (7–14) (BBN) at 15 mg/kg or RGD at 10 mg/kg + BBN at 15 mg/kg and 3.7 MBq of ^{68}Ga-NOTA-RGD-BBN, and 5-min static PET scans were then

acquired at 1 h after injection (n=3 per group). For each microPET scan, regions of interest (ROIs) were drawn over the tumor, normal tissue, and major organs using vendor software ASI Pro 5.2.4.0 on decay-corrected whole-body coronal images. The maximum radioactivity concentrations (accumulation) within a tumor or an organ were obtained from mean pixel values within the multiple ROI volume, and were converted to megabecquerels per milliliter per minute using a conversion factor. , These values were then divided by the administered activity to obtain (assuming a tissue density of 1 g/ml) an image ROI-derived percent injected dose per gram (%ID/g).

Biodistribution studies

Male athymic nude mice bearing PC-3 xenografts were injected with 0.74 MBq (20 μCi) of ^{68}Ga-NOTA-RGD-BBN to evaluate the distribution of the tracer in the tumor tissues and major organs. At 0.5 h and 1 h after injection of the tracer, the tumor-bearing mice were killed and dissected. Blood, tumor, major organs, and tissues were collected and wet-weighed. The radioactivity in the tissue was measured by γ counter (Packard). The results are presented as percentage injected dose per gram of tissue (%ID/g). For each mouse, the radioactivity of the tissue samples was calibrated against a known aliquot of the injectate and normalized to a body mass of 20 g. Values were expressed as mean±SD for groups of four animals (n=4 per group).

Immunofluorescence staining

Immunofluorescence staining studies were performed as we have previously reported [4] with some modifications. Briefly, frozen PC-3 tumor and organ tissue slices (5-μm thickness) from the tumor-bearing nude mice were fixed with ice-cold acetone, rinsed with PBS and blocked with 10% goat serum for 30 min at room temperature. The slices were incubated with goat anti-GRPR antibody (1:100; Santa Cruz Biotechnology, Santa Cruz, CA), humanized antihuman integrin $\alpha_v\beta_3$ antibody Abegrin [4] (20 μg/ml), or hamster anti-β_3 antibody (1:100; BD Biosciences, San Jose, CA) for 1 h at room temperature and then visualized with FITC-conjugated donkey antigoat, cy3-conjugated donkey antihuman or Cy3-conjugated goat antihamster secondary antibodies (1:200; Jackson ImmunoResearch Laboratories, West Grove, PA), respectively. For the overlaid staining of CD31 and murine β_3, PC-3 tumor slices were incubated with rat antimouse CD31 antibody (1:100; BD Biosciences) and hamster anti-β_3 antibody (1:100; BD Biosciences) and then visualized with Cy3-conjugated goat antirat and FITC-conjugated goat antihamster secondary antibody (1:200; Jackson ImmunoResearch Laboratories).

Statistical analysis

Quantitative data are expressed as means±SD. Means were compared using one-way analysis of variance (ANOVA) and a Student's t test. P values <0.05 were considered statistically significant.

Results

Chemistry and radiochemistry

The NOTA conjugates of RGD, BBN and RGD-BBN (Fig. 1a) were analyzed by both analytical HPLC and mass spectroscopy to confirm the identity of the products. ^{68}Ga was eluted from a ^{68}Ge/^{68}Ga generator and used directly for the reaction after adjusting the pH. The labeling was done within 30 min, with a decay-corrected yield ranging from 90% to 95% and a radiochemical purity of more than 98%.

Cell binding assay

The integrin $\alpha_v\beta_3$ receptor-binding affinities of RGD-BBN, NOTA-RGD-BBN were determined by performing competitive binding assay with ^{125}I-c(RGDyK) as the radioligand. Cyclic RGD peptide c(RGDyK) and BBN were also added for comparison. RGD-BBN and NOTA-RGD-BBN inhibited the binding of ^{125}I-c(RGDyK) to integrin-expressing U87MG cells in a concentration-dependent manner. The IC_{50} values for RGD-BBN, NOTA-RGD-BBN and c(RGDyK) were 17.91±5.70 nM, 22.57±6.68 nM, and 11.19±4.21 nM, respectively (Fig. 1b). BBN did not show significant binding inhibition of ^{125}I-c(RGDyK). The binding affinities of RGD-BBN, NOTA-RGD-BBN, and Aca-BBN(7–14) for GRPR were evaluated using GRPR-positive PC-3 cells with ^{125}I-[Tyr^4]BBN as the radioligand. The results of the cell-binding assay were plotted as sigmoid curves for the displacement of ^{125}I-[Tyr^4]BBN from PC-3 cells as a function of increasing concentration of BBN analogs. The IC_{50} values were determined to be 67.92±4.97 nM for RGD-BBN, 55.89±4.23 nM for NOTA-RGD-BBN, and 78.96±4.86 nM for BBN on PC-3 cells. RGD did not show significant binding inhibition of ^{125}I-[Tyr^4]BBN with GRPR (Fig. 1c). The IC_{50} values from these two sets of experiments suggest that RGD-BBN possessed comparable GRPR and integrin $\alpha_v\beta_3$ receptor-binding affinities with the corresponding unmodified monomers. Conjugation of NOTA had little effect on the integrin and GRPR receptor-binding characteristics. It should be noted that the IC_{50} value depends largely on the radioligands, tumor cells and reaction conditions used in the in vitro competitive assay, so caution should be taken when directly comparing the IC_{50}

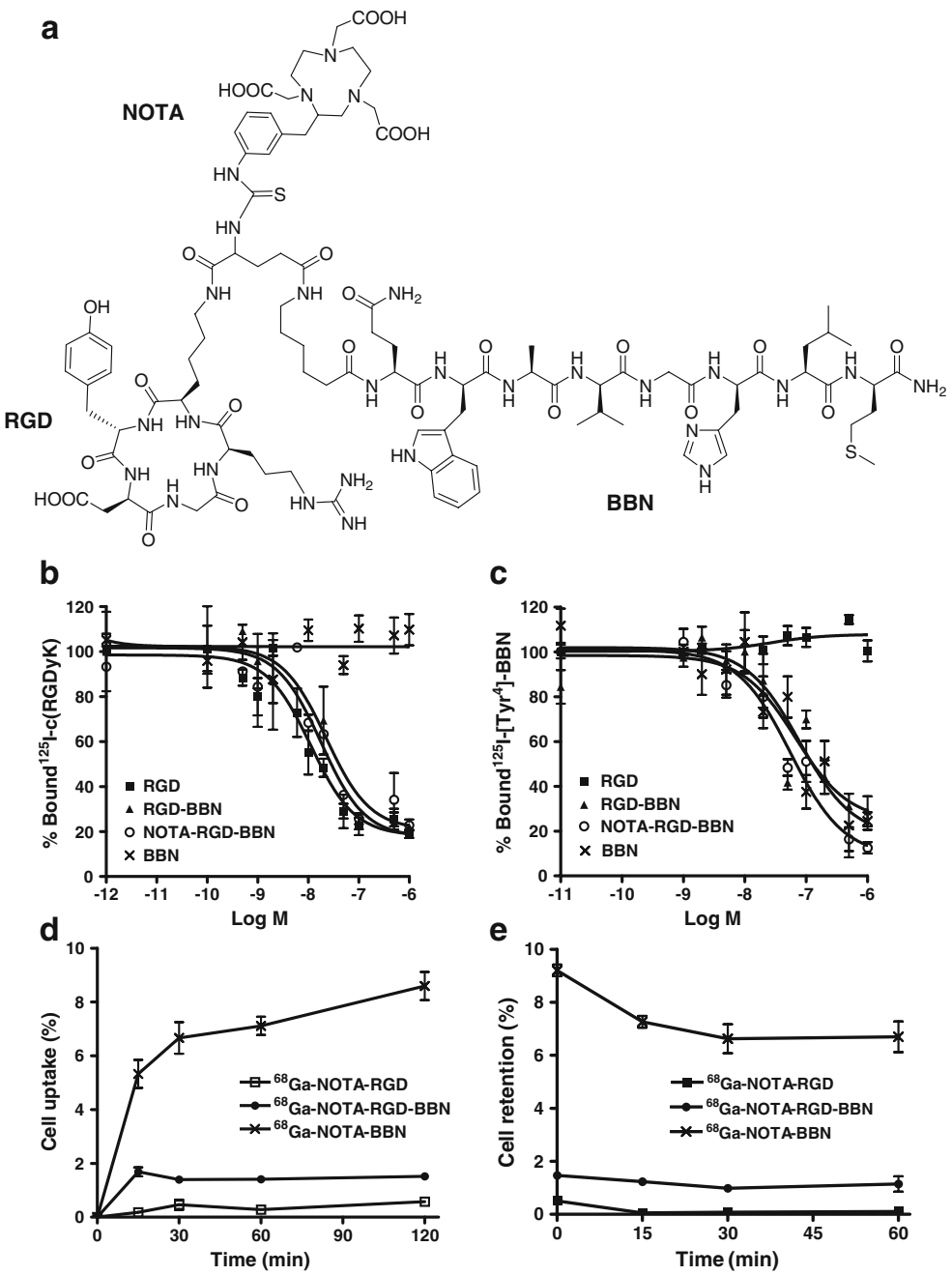

Fig. 1 **a** Chemical structure of NOTA-RGD-BBN heterodimer. **b** Inhibition of ^{125}I-c(RGDyK) binding to integrin $\alpha_v\beta_3$ on U87MG cells by c(RGDyK) (RGD), RGD-BBN, NOTA-RGD-BBN and Aca-BBN(7–14) (BBN) (n=3, mean±SD). **c** Inhibition of ^{125}I-[Tyr4]-BBN (GRPR-specific) binding to GRPR on PC-3 cells by Aca-BBN(7–14) (BBN), RGD-BBN, NOTA-RGD-BBN, and c(RGDyK) (RGD) (n=3, mean±SD). **d** Cell uptake assay of ^{68}Ga-NOTA-RGD-BBN, ^{68}Ga-NOTA-RGD, and ^{68}Ga-NOTA-BBN in PC-3 tumor cells (n=3, mean±SD). **e** Cell efflux assay of ^{68}Ga-NOTA-RGD-BBN, ^{68}Ga-NOTA-RGD, and ^{68}Ga-NOTA-BBN in PC-3 tumor cells (n=3, mean±SD)

values of the tracers reported here with those reported in the literatures.

Cell uptake and efflux studies

The cell uptake and efflux of ^{68}Ga-NOTA-RGD-BBN were evaluated in studies in PC-3 tumor cells that express high levels of GRPR and moderate levels of integrin $\alpha_V\beta_3$ (2.7×10^6 GRPRs per cell and 2.76×10^3 integrins per cell) [29, 30]. ^{68}Ga-NOTA-BBN had rather rapid and high cell uptake (Fig. 1d), which is similar to those of ^{64}Cu and ^{18}F labeled BBN tracers that have been previously reported [31, 32]. ^{68}Ga-NOTA-RGD had relatively low cell uptake, which is possibly due to the low integrin receptor density of PC-3 cells. The cell uptake curve of ^{68}Ga-NOTA-RGD-BBN was between those of ^{68}Ga-NOTA-BBN and ^{68}Ga-NOTA-RGD. ^{68}Ga-NOTA-RGD-BBN uptake reached a plateau at 15 min incubation (1.69±0.29%AD) and remained at a similar level for up to 2 h. Note that the cell uptake protocol used in this study did not distinguish between cell surface-bound and internalized activity. The cell retention of the three tracers also showed the order BBN > RGD-BBN > RGD. The cell-associated RGD peptide was undetectable after 15 min. The cell retention of

both ^{68}Ga-NOTA-BBN and ^{68}Ga-NOTA-RGD-BBN decreased with time. At 60 min, the cell-associated tracers were 6.70±1.00%AD for BBN, 1.14±0.50%AD for RGD-BBN and 0.10±0.13%AD for RGD, respectively (Fig. 1e).

MicroPET imaging

Representative coronal microPET images of PC-3 tumor-bearing mice (n=4 per group) at different times after intravenous injection of 3.7 MBq (100 μCi) of ^{68}Ga-NOTA-RGD-BBN are shown in Fig. 2a. ^{68}Ga-NOTA-BBN and ^{68}Ga-NOTA-RGD were used as controls. The tumors after injection of ^{68}Ga-NOTA-RGD-BBN and ^{68}Ga-NOTA-BBN were clearly visible with high contrast in relation to the contralateral background at all time points measured from 30 to 120 min. ^{68}Ga-NOTA-RGD showed low uptake in PC-3 tumors due to the relatively low expression of integrin $\alpha_v\beta_3$ of PC-3 cells and low affinity of monomer RGD peptide with integrin. Prominent uptake of ^{68}Ga-NOTA-RGD-BBN was also observed in the kidneys at early time points, suggesting that this tracer is mainly excreted through the renal-urinary route. Tumor and major organ activity accumulation in the microPET scans was quantified by measuring the ROIs that encompassed the

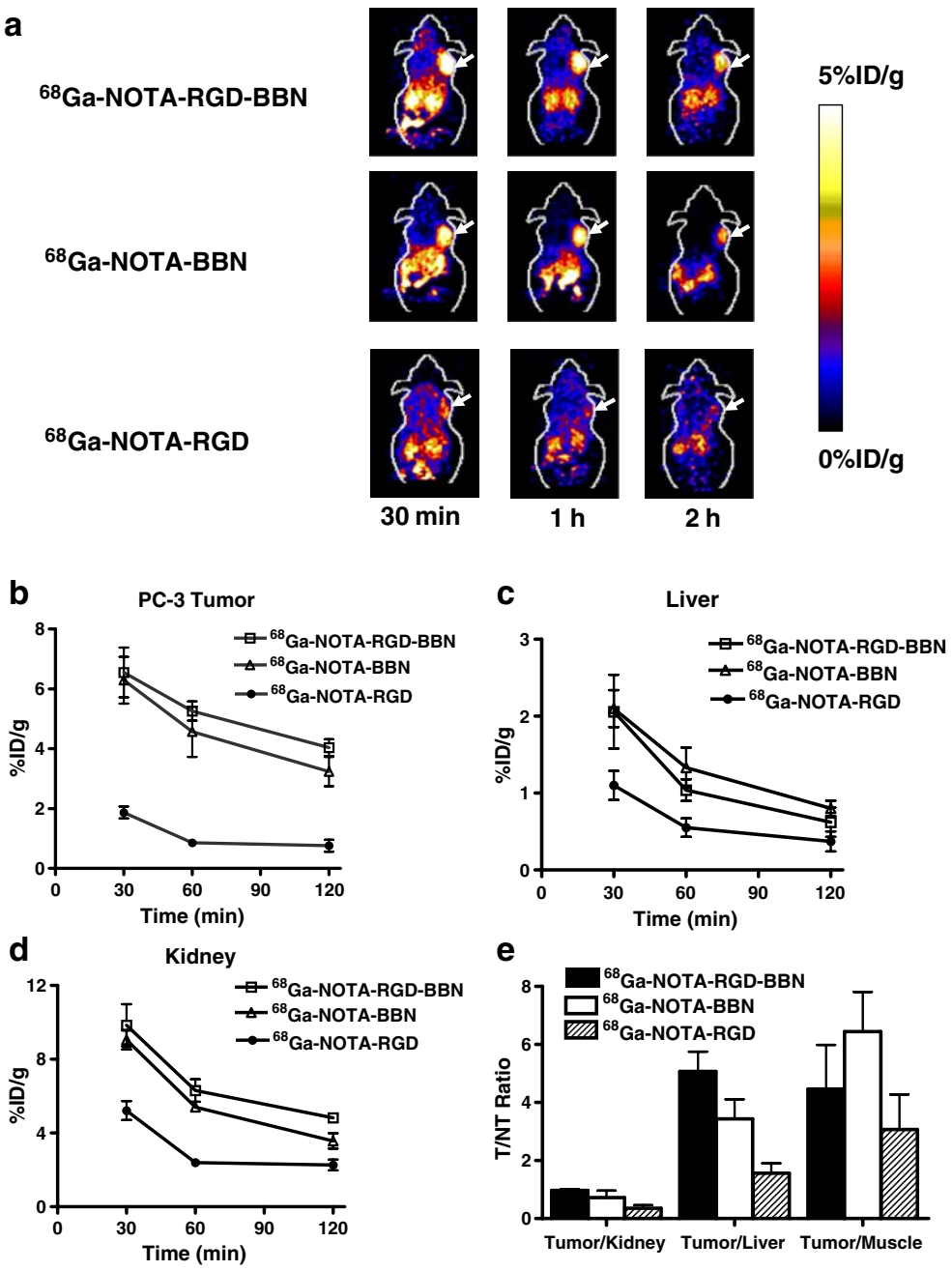

Fig. 2 **a** Decay-corrected whole-body coronal microPET images of PC-3 tumor-bearing mice at 30, 60 and 120 min after injecting 3.7 MBq (100 μCi) of ^{68}Ga-NOTA-RGD-BBN, ^{68}Ga-NOTA-BBN, or ^{68}Ga-NOTA-RGD. The images shown are 5-min static scans of a single mouse, which is representative of the four mice tested in each group (*arrows* PC-3 tumor). **b–d** Comparison between the quantified uptake of ^{68}Ga-NOTA-RGD-BBN, ^{68}Ga-NOTA-BBN, and ^{68}Ga-NOTA-RGD in PC-3 tumor (**b**), liver (**c**), and kidneys (**d**) (n=4 per group, means±SD). **e** Comparison of tumor to kidney, liver and muscle ratios of ^{68}Ga-NOTA-RGD-BBN, ^{68}Ga-NOTA-BBN, and ^{68}Ga-NOTA-RGD at 60 min after injection of 3.7 MBq (100 μCi) tracer in PC-3 tumor-bearing mice (n=4 per group, means±SD)

entire organ on the coronal images. The tumor uptake of ^{68}Ga-NOTA-RGD-BBN was determined to be 6.55±0.83, 5.26±0.32, and 4.04±0.28%ID/g at 30, 60, and 120 min (Fig. 2b). The liver uptake was very low, the highest being about 2%ID/g at 30 min after injection (Fig. 2c).

A comparison of the kinetics of ^{68}Ga-labeled RGD-BBN, BBN and RGD tracers in the tumor, liver and kidneys is shown in Fig. 2b–d. The tumor uptake of ^{68}Ga-labeled RGD-BBN was significantly higher than that of BBN and RGD tracers at all time points examined ($p<0.05$), except that there was no significant difference at 30 min after injection compared with BBN. The tumor uptake of BBN tracer was also higher than that of RGD at all time points, which was mainly due to a high expression of GRPR and low expression of integrin in the PC-3 tumors. The liver uptakes of the three tracers were all very low, with the highest being 2%ID/g for BBN at 30 min after injection. The liver uptake of RGD was somewhat lower than that of BBN and RGD-BBN. The kidney uptake of ^{68}Ga-NOTA-RGD-BBN and ^{68}Ga-NOTA-BBN was significantly higher than that of RGD at all time points ($p<0.05$). The kidney uptake of RGD-BBN was slightly higher than that of BBN at all time points. Due to the rapid clearance of the tracers, the T/NT ratios increased with time for all three tracers. The tumor/kidney, tumor/liver and tumor/muscle ratios of the three tracers are shown for 1 h after injection in Fig. 2e. The tumor/kidney and tumor/liver ratios of RGD-BBN were significantly higher than those of BBN and RGD ($p<0.01$). The tumor/muscle ratios followed the order BBN > RGD-BBN > RGD ($n=4$ per group).

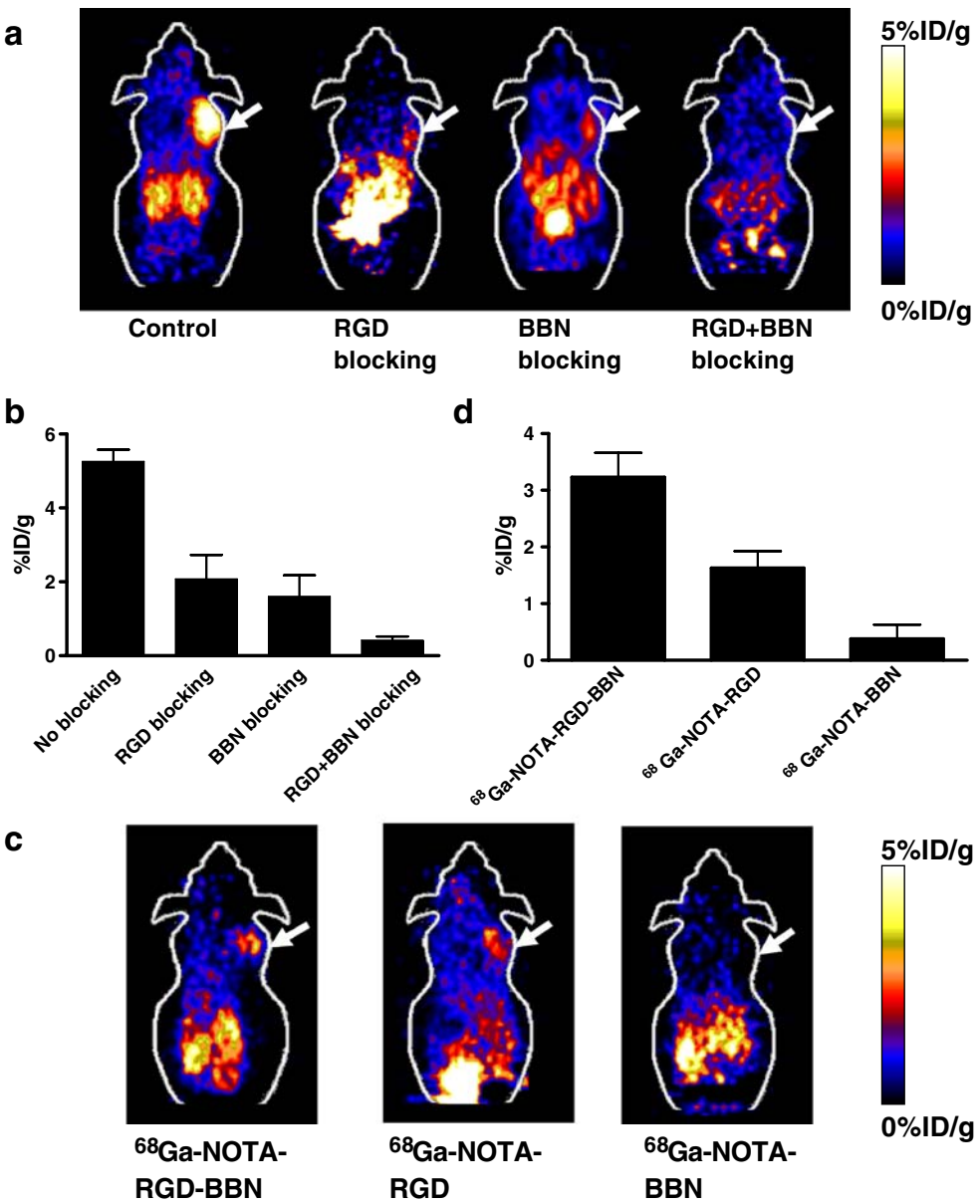

Fig. 3 **a** Decay-corrected whole-body coronal microPET images of PC-3 tumor-bearing mice at 1 h after injection of 3.7 MBq (100 μCi) of ^{68}Ga-NOTA-RGD-BBN and a blocking dose of c (RGDyK) (10 mg/kg), BBN (15 mg/kg), or RGD (10 mg/kg) and BBN (15 mg/kg) ($n=3$ or 4 per group). **b** Comparison between the quantified uptake of ^{68}Ga-NOTA-RGD-BBN in PC-3 tumor with or without preinjection of a blocking dose of peptide (RGD, BBN, or RGD + BBN). Data are expressed as means %ID/g +SD ($n=3$ or 4 per group). **c** Decay-corrected whole-body coronal microPET images of MDA-MB-435 tumor-bearing mice at 60 min after injection of 3.7 MBq (100 μCi) of ^{68}Ga-NOTA-RGD-BBN, ^{68}Ga-NOTA-BBN, or ^{68}Ga-NOTA-RGD. Images shown are 5-min static scans of a single mouse, which is representative of the four mice tested in each group (*arrows* MDA-MB-435 tumor). **d** Comparison of the quantified tumor uptake of ^{68}Ga-NOTA-RGD-BBN, ^{68}Ga-NOTA-RGD, and ^{68}Ga-NOTA-BBN in MDA-MB-435 tumor-bearing mice. Data are expressed as means %ID/g +SD ($n=4$ per group)

The in vivo integrin and GRPR dual receptor binding property of ^{68}Ga-NOTA-RGD-BBN was confirmed by several blocking studies (Fig. 3a, b). Representative coronal images of PC-3 tumor mice at 1 h after injection of ^{68}Ga-NOTA-RGD-BBN in the presence of RGD (10 mg/kg), BBN (15 mg/kg), or both RGD and BBN (10 mg/kg of RGD and 15 mg/kg of BBN) are shown in Fig. 3a. The tumor uptake of ^{68}Ga-NOTA-RGD-BBN was partially inhibited by RGD (from 5.26±0.32%ID/g to 2.08±0.65% ID/g) and by BBN (from 5.26±0.32%ID/g to 1.61±0.57% ID/g). However, when ^{68}Ga-NOTA-RGD-BBN was coadministered with RGD and BBN, the tumor uptake was significantly inhibited to the background level (0.42± 0.10%ID/g; Fig. 3b, n=3 per group).

The in vivo behaviors of ^{68}Ga-NOTA-RGD-BBN, ^{68}Ga-NOTA-BBN, and ^{68}Ga-NOTA-RGD were also tested in MDA-MB-435 tumor model, which expresses moderate levels of integrin $\alpha_v\beta_3$, but undetectable levels of GRPR (based on radioligand binding assays, unpublished data). As shown in Fig. 3c, the BBN tracer did not show significant uptake in the MDA-MB-435 tumors, while RGD tracer showed good tumor contrast at 1 h after injection. ^{68}Ga-NOTA-RGD-BBN also showed clear tumor uptake due to the integrin recognition of RGD-BBN in vivo. At 60 min after injection, the tumor uptake values of RGD-BBN, BBN, and RGD were 3.23±0.86, 0.38±0.50 and 1.63± 0.59%ID/g, respectively (Fig. 3d).

The tumor targeting property of ^{68}Ga-NOTA-RGD-BBN in PC-3 tumor-bearing mice was also evaluated by a 30-min dynamic microPET scan followed by 5-min static scans at 1 h and 2 h after injection. Representative coronal images and quantified %ID/g by ROI analysis at different time points after injection are shown in Fig. 4a, b. High tumor uptake was observed as early as 5 min after injection. The PC-3 tumor uptake was 5.56, 6.68, 6.70, 4.47 and 3.75% ID/g at 5, 15, 30, 60 and 120 min after injection, respectively. With clearance of the tracer from the blood and normal organs, the tumor contrast increased with time. The tracer was excreted mainly through the kidneys, as evidenced by the higher renal uptake at early time points and excretion via the bladder. The kidney uptake reached a peak at about 10 min after injection and then decreased with time. At 120 min after injection, the tumor uptake of the tracer was higher than that in any other normal organ (Fig. 4b).

Biodistribution studies

The biodistribution study of ^{68}Ga-NOTA-RGD-BBN was performed in nude mice bearing PC-3 tumors. Each mouse was injected with 0.74 MBq (20 μCi) of ^{68}Ga-NOTA-RGD-BBN and then killed at 0.5 h and 1 h after injection (n=4 per group). As shown in Fig. 5, the tracer uptake decreased from 0.5 h to 1 h in the PC-3 tumors and all the

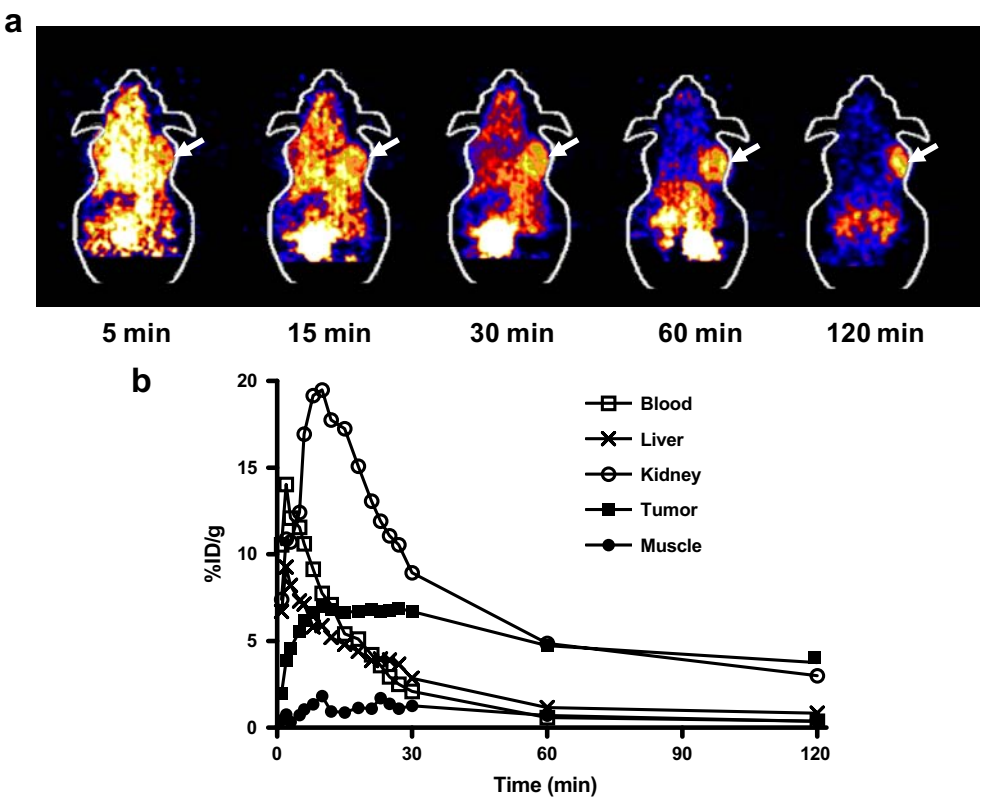

Fig. 4 Dynamic microPET imaging. **a** Decay-corrected whole-body coronal microPET images of a PC-3 tumor-bearing mouse from a 30-min dynamic scan and two static scans at 1 h and 2 h after injection of 3.7 MBq (100 μCi) of ^{68}Ga-NOTA-RGD-BBN (*arrows* PC-3 tumor). **b** Quantified time–%ID/g curves of tumor and major organs after injection of 3.7 MBq (100 μCi) of ^{68}Ga-NOTA-RGD-BBN in a PC-3 tumor-bearing mouse

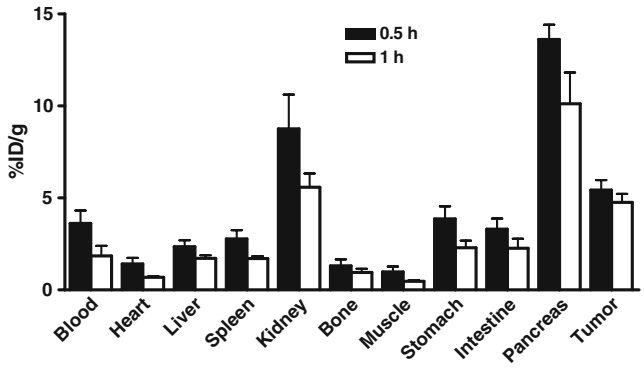

Fig. 5 Biodistribution of ^{68}Ga-NOTA-RGD-BBN (0.74 MBq per mouse) in PC-3 tumor-bearing nude mice at 0.5 h and 1 h after injection. Data are expressed as means %ID/g +SD (n=4 per group)

examined organs. For example, the tumor uptake was 5.43± 0.54%ID/g at 0.5 h and 4.76±0.46%ID/g at 1 h. The kidney uptake decreased from 8.76±1.83% ID/g at 0.5 h after injection to 5.58±0.75%ID/g at 1 h after injection. The tumor uptake of ^{68}Ga-NOTA-RGD-BBN was significantly higher than that in the blood and normal organs, such as the heart, liver, spleen, bone, and muscle at 0.5 h and 1 h ($p<$ 0.01). The tracer also showed high uptake in the pancreas, stomach and intestine due to the high GPPR expression in these organs.

Immunofluorescent staining

The expression of GRPR and integrin $\alpha_v\beta_3$ in the PC-3 tumor and normal organs was tested by immunofluorescent staining using anti-GRPR, anti-human $\alpha_v\beta_3$ and anti-murine β_3 antibodies. PC-3 tumors were found to be positive for GRPR, human $\alpha_v\beta_3$ and murine β_3 (Fig. 6a). Because RGD peptide can bind both human and murine integrin, while BBN can bind GRPR, PC-3 tumors possess recognition sites for both RGD and BBN. In contrast, normal organs such as the liver, kidneys and muscle do not express GRPR, while the small intestine and stomach express high levels of GRPR around the lumen. Some other normal organs also express low levels of murine β_3 (Supplementary Material Fig. 1). Overlaid staining of CD31 and murine β_3 in PC-3 tumors is shown in Fig. 6b. Most of the murine integrin β_3-positive areas were also CD31-positive, indicating that the expression of murine integrin $\alpha_v\beta_3$ was derived from the tumor vasculature.

Discussion

The recent introduction of ^{68}Ga into clinical practice represents the beginning of the development of a PET imaging probe that is not dependent on the availability of a medical cyclotron [33]. ^{68}Ga has the physical property of high positron yield reaching 89% of all disintegrations, which is suitable for PET imaging. Its short physical half-life of 68 min matches the biological half-lives of many peptides and other small molecules owing to their fast blood clearance, quick penetration and rapid target localization. In this study, we investigated the in vitro and in vivo characteristics of ^{68}Ga-labeled RGD-BBN heterodimeric peptide in a dual integrin- and GRPR-positive PC-3 tumor model.

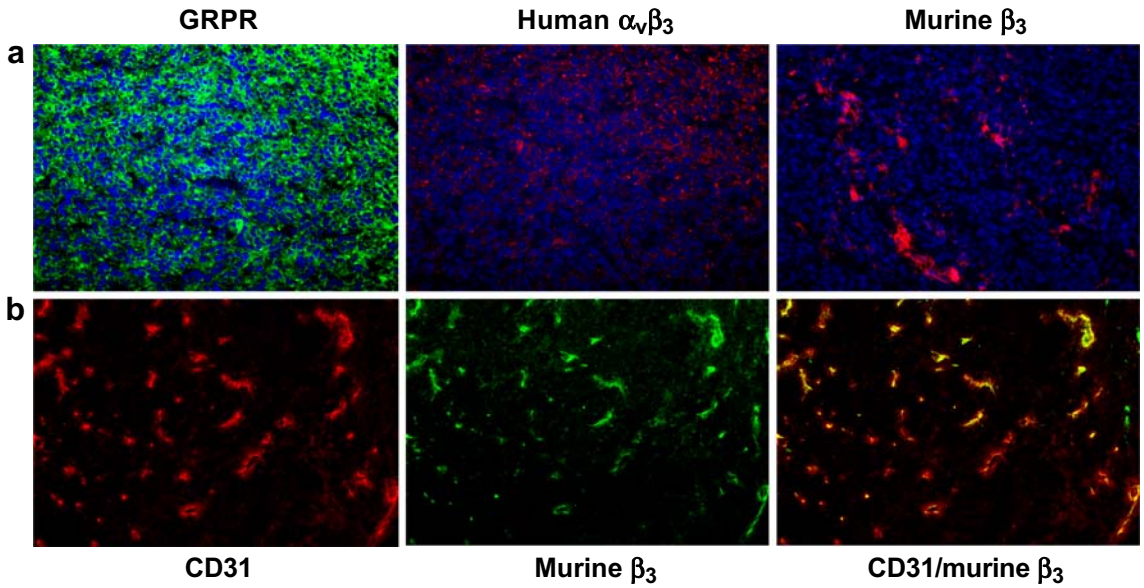

Fig. 6 **a** Immunofluorescent staining of GRPR, human integrin $\alpha_v\beta_v$, and murine integrin β_3 in PC-3 tumor tissue. **b** Overlaid staining of murine CD31 and murine integrin β_3 in PC-3 tumor tissue

To be a dual functional tracer, each binding motif of the heterodimer must maintain its own function. Our receptor-binding assay data demonstrated that the binding affinities of RGD-BBN and NOTA-RGD-BBN were similar to that of Aca-BBN(7–14) for GRPR binding and c(RGDyK) for integrin $\alpha_v\beta_3$ binding, indicating that the RGD-BBN heterodimer can bind both integrin and GRPR in vitro. ^{68}Ga-NOTA-RGD-BBN showed lower uptake than ^{68}Ga-NOTA-BBN, but higher uptake than ^{68}Ga-NOTA-RGD in PC-3 tumor cells. This may be due to the facts that PC-3 cells have higher numbers of GRPR than integrin, and that the RGD-integrin complex does not tend to internalize into the cells. The internalization of BBN in the RGD-BBN heterodimer was significantly hampered by the recognition of the RGD motif with the cell-surface integrin receptor.

The in vivo behavior of ^{68}Ga-NOTA-RGD-BBN was tested in a PC-3 tumor model using microPET. The PC-3 tumor uptake of ^{68}Ga-NOTA-RGD-BBN was slightly higher than that of ^{68}Ga-NOTA-BBN, but much higher than that of ^{68}Ga-NOTA-RGD at all time points examined (Fig. 2b). It is easy to explain the higher tumor uptake of ^{68}Ga-NOTA-RGD-BBN as compared to ^{68}Ga-NOTA-RGD as PC-3 tumors express relatively high levels of GRPR but low levels of integrin (Fig. 6a). However, the insignificant difference in PC-3 tumor uptake of ^{68}Ga-NOTA-RGD-BBN and ^{68}Ga-NOTA-BBN seemingly conflicts with the in vitro cell uptake results that ^{68}Ga-NOTA-BBN had much higher uptake and retention in PC-3 cells. There are several possible reasons for such an in vitro and in vivo discrepancy. First, in the nude mouse model, the PC-3 tumor vasculature also expresses a high levels of murine integrin β_3 (Fig. 6a) which can be recognized by the RGD motif, while the PC-3 tumor cells in vitro do not express murine integrin receptors. The increased integrin receptor numbers may be partially responsible for the slightly increased tumor uptake of ^{68}Ga-NOTA-RGD-BBN in vivo. Second, the signal increase of ^{68}Ga-NOTA-RGD-BBN over any of the counterpart monomeric tracers may represent a synergistic interaction between the two binding motifs in the heterodimer. It is possible that the binding of one motif, even if only temporarily, could first capture the ^{68}Ga-NOTA-RGD-BBN to the target surface or slow down the moving of the ^{68}Ga-NOTA-RGD-BBN, allowing the second binding motif to also attach to the tumor, thereby increasing the overall binding and the probability of ^{68}Ga-NOTA-RGD-BBN adhering to the tumor. Third, because the RGD motif can recognize murine integrin β_3 expressed on the tumor vasculature (Fig. 6b), it is possible that the ^{68}Ga-NOTA-RGD-BBN in the circulation would first bind tumor vascular integrin. As the binding affinity of RGD monomer is relatively low, the tracer accumulated around the tumor vessel may dissociate from the loosely bound integrin receptors, diffuse into the extracellular matrix and rebind to the tumor cells that express both GRPR and integrin $\alpha_v\beta_3$.

One of the main drawbacks of BBN-based radiotracers is their unfavorable hepatobiliary excretion, which usually results in high intestinal uptake. For example, in this study, as shown in Fig. 2a, ^{68}Ga-NOTA-BBN exhibited high and persistent intestinal accumulation, which is presumably due to the high lipophilicity of ^{68}Ga-NOTA-BBN. In contrast, ^{68}Ga-NOTA-RGD-BBN was excreted mainly through the kidneys as evidenced by the dynamic curve shown in Fig. 4b. The altered in vivo kinetics of ^{68}Ga-NOTA-RGD-BBN compared with ^{68}Ga-NOTA-BBN may be attributed to their differences in molecular size and charge, hydrophilicity, and metabolic stability. Overall, the heterodimeric tracer significantly reduced the intestinal accumulation of radioactivity, making the tracer more suitable for imaging of abdominal cancer than BBN analogs.

Compared with our previously reported ^{18}F-labeled RGD-BBN heterodimers [22, 24], the production of ^{68}Ga-NOTA-RGD-BBN is much easier and does not need an on-site cyclotron, which allows possible kit formulation and widespread availability. The PC-3 tumor uptake of ^{68}Ga-NOTA-RGD-BBN (6.55±0.83, 5.26±0.32, and 4.04±0.28%ID/g at 30, 60, and 120 min, respectively) was significantly higher than that of ^{18}F-FB-PEG$_3$-RGD-BBN (6.35±2.52, 4.41±0.71, and 2.47±0.81%ID/g at 30, 60, and 120 min, respectively [24]) at 60 min after injection ($p<0.05$). The higher tumor uptake of the ^{68}Ga-labeled RGD-BBN is likely due to the internalization and effective trapping of radiometal inside the tumor cells as compared to ^{18}F-labeled tracers, which is supported by cell efflux studies. After allowing efflux for 1 h, the efflux ratio was about 40% for ^{18}F-labeled RGD-BBN [22], but only about 20% for ^{68}Ga-NOTA-RGD-BBN. The cellular uptake of ^{68}Ga-NOTA-BBN was much higher than that of ^{68}Ga-NOTA-RGD-BBN (Fig. 1d), so cell-trapped ^{68}Ga would be higher for ^{68}Ga-NOTA-BBN than for ^{68}Ga-NOTA-RGD-BBN. This possibly explains why ^{68}Ga-NOTA-BBN also showed much higher tumor uptake than ^{18}F-labeled BBN tracer [22].

The dual receptor binding specificity of ^{68}Ga-NOTA-RGD-BBN in vivo was confirmed by the blocking studies. Either Aca-BBN(7–14) or cyclic RGD peptide c(RGDyK) can only partially inhibit the uptake of ^{68}Ga-NOTA-RGD-BBN in the PC-3 tumor, as the BBN motif of the ^{68}Ga-NOTA-RGD-BBN can bind to the GRPR when integrin is blocked by RGD, and the RGD motif of the ^{68}Ga-NOTA-RGD-BBN can bind to the integrin when GRPR is blocked by BBN. The advantage of dual receptor binding of the heterodimer tracer is obvious when only one receptor type is overexpressed in a tumor model. For example, in the MDA-MB-435 tumor model, which expresses a moderate level of integrin $\alpha_v\beta_3$ but no GRPR, ^{68}Ga-NOTA-BBN was

unable to detect the tumors because it only recognizes GRPR. In contrast, ^{68}Ga-NOTA-RGD and ^{68}Ga-NOTA-RGD-BBN had a clear tumor uptake due to the function of RGD (Fig. 3c, d). The MDA-MB-435 tumor uptake of ^{68}Ga-NOTA-RGD-BBN was even higher than that of ^{68}Ga-NOTA-RGD tumor, which may have resulted from the improved in vivo kinetics and increased circulation half-life of ^{68}Ga-NOTA-RGD-BBN over ^{68}Ga-NOTA-RGD.

In the ^{68}Ga-NOTA-RGD-BBN heterodimeric peptide, the RGD and BBN motifs were linked through a glutamic acid. Due to the short length of the linker, it is impossible for the RGD and BBN motifs to bind both integrin and GRPR simultaneously. Therefore, in future it would be interesting to investigate the effects of linkers of different lengths, solubility, lipophilicity, and flexibility on the in vitro and in vivo behaviors of the heterodimeric peptides. The design of heteromultimeric tracers that recognize other tumor targets is also worth further investigation for tumor-targeted imaging and therapy.

In conclusion, we have described the design and synthesis of ^{68}Ga-labeled RGD-BBN heterodimer peptide containing both RGD and BBN motifs for dual integrin- and GRPR-targeted tumor imaging. ^{68}Ga-NOTA-RGD-BBN exhibited dual receptor targeting properties both in vitro and in vivo. The high affinity and specificity and improved pharmacokinetics of the ^{68}Ga-labeled RGD-BBN heterodimer make it a promising agent for molecular imaging of tumors with both or either receptor expression pattern. The heterodimer and heteromultimer strategy may also provide general methods of developing tumor-targeted imaging probes and therapeutic agents.

Acknowledgments This work was supported, in part, by the National Cancer Institute (NCI R01 CA119053, R21 CA121842, P50 CA114747 and U54 CA119367). We thank Drs. Shuanglong Liu and Kai Chen for excellent technical support. Z. Liu would like to acknowledge the China Scholarship Council (CSC) for partial financial support during his study at Stanford University.

References

1. Okarvi SM. Peptide-based radiopharmaceuticals: future tools for diagnostic imaging of cancers and other diseases. Med Res Rev 2004;24:357–97. doi:10.1002/med.20002.
2. Chen X, Liu S, Hou Y, Tohme M, Park R, Bading JR, et al. MicroPET imaging of breast cancer αv-integrin expression with 64Cu-labeled dimeric RGD peptides. Mol Imaging Biol 2004;6:350–9. doi:10.1016/j.mibio.2004.06.004.
3. Li ZB, Chen K, Chen X. 68Ga-labeled multimeric RGD peptides for microPET imaging of integrin αvβ3 expression. Eur J Nucl Med Mol Imaging 2008;35:1100–8. doi:10.1007/s00259-007-0692-y.
4. Wu Z, Li ZB, Cai W, He L, Chin FT, Li F, et al. 18F-labeled mini-PEG spacered RGD dimer (18F-FPRGD2): synthesis and micro-PET imaging of αvβ3 integrin expression. Eur J Nucl Med Mol Imaging 2007;34:1823–31. doi:10.1007/s00259-007-0427-0.
5. Liu S, Hsieh WY, Jiang Y, Kim YS, Sreerama SG, Chen X, et al. Evaluation of a 99mTc-labeled cyclic RGD tetramer for noninvasive imaging integrin αvβ3-positive breast cancer. Bioconjug Chem 2007;18:438–46. doi:10.1021/bc0603081.
6. Beer AJ, Grosu AL, Carlsen J, Kolk A, Sarbia M, Stangier I, et al. [18F]galacto-RGD positron emission tomography for imaging of αvβ3 expression on the neovasculature in patients with squamous cell carcinoma of the head and neck. Clin Cancer Res 2007;13:6610–6. doi:10.1158/1078-0432.CCR-07-0528.
7. Beer AJ, Haubner R, Sarbia M, Goebel M, Luderschmidt S, Grosu AL, et al. Positron emission tomography using [18F]Galacto-RGD identifies the level of integrin αvβ3 expression in man. Clin Cancer Res 2006;12:3942–9. doi:10.1158/1078-0432.CCR-06-0266.
8. Haubner R, Weber WA, Beer AJ, Vabuliene E, Reim D, Sarbia M, et al. Noninvasive visualization of the activated αvβ3 integrin in cancer patients by positron emission tomography and [18F] Galacto-RGD. PLoS Med 2005;2:e70. doi:10.1371/journal.pmed.0020070.
9. Kenny LM, Coombes RC, Oulie I, Contractor KB, Miller M, Spinks TJ, et al. Phase I trial of the positron-emitting Arg-Gly-Asp (RGD) peptide radioligand 18F-AH111585 in breast cancer patients. J Nucl Med 2008;49:879–86. doi:10.2967/jnumed.107.049452.
10. Cornelio DB, Roesler R, Schwartsmann G. Gastrin-releasing peptide receptor as a molecular target in experimental anticancer therapy. Ann Oncol 2007;18:1457–66. doi:10.1093/annonc/mdm058.
11. Dimitrakopoulou-Strauss A, Hohenberger P, Haberkorn U, Macke HR, Eisenhut M, Strauss LG. 68Ga-labeled bombesin studies in patients with gastrointestinal stromal tumors: comparison with 18F-FDG. J Nucl Med 2007;48:1245–50. doi:10.2967/jnumed.106.038091.
12. Van de Wiele C, Phonteyne P, Pauwels P, Goethals I, Van den Broecke R, Cocquyt V, et al. Gastrin-releasing peptide receptor imaging in human breast carcinoma versus immunohistochemistry. J Nucl Med 2008;49:260–4. doi:10.2967/jnumed.107.047167.
13. Scheffel U, Pomper MG. PET imaging of GRP receptor expression in prostate cancer. J Nucl Med 2004;45:1277–8.
14. de Visser M, van Weerden WM, de Ridder CM, Reneman S, Melis M, Krenning EP, et al. Androgen-dependent expression of the gastrin-releasing peptide receptor in human prostate tumor xenografts. J Nucl Med 2007;48:88–93.
15. Liu S. Radiolabeled multimeric cyclic RGD peptides as integrin αvβ3 targeted radiotracers for tumor imaging. Mol Pharm 2006;3:472–87. doi:10.1021/mp060049x.
16. Jia B, Liu Z, Shi J, Yu Z, Yang Z, Zhao H, et al. Linker effects on biological properties of 111In-labeled DTPA conjugates of a cyclic RGDfK dimer. Bioconjug Chem 2008;19:201–10. doi:10.1021/bc7002988.
17. Smith CJ, Volkert WA, Hoffman TJ. Radiolabeled peptide conjugates for targeting of the bombesin receptor superfamily subtypes. Nucl Med Biol 2005;32:733–40. doi:10.1016/j.nucmedbio.2005.05.005.
18. Janssen ML, Oyen WJ, Dijkgraaf I, Massuger LF, Frielink C, Edwards DS, et al. Tumor targeting with radiolabeled αvβ3 integrin binding peptides in a nude mouse model. Cancer Res 2002;62:6146–51.
19. Dijkgraaf I, Boerman OC, Oyen WJ, Corstens FH, Gotthardt M. Development and application of peptide-based radiopharmaceuticals. Anticancer Agents Med Chem 2007;7:543–51.
20. Li ZB, Cai W, Cao Q, Chen K, Wu Z, He L, et al. 64Cu-labeled tetrameric and octameric RGD peptides for small-animal PET of tumor αvβ3 integrin expression. J Nucl Med 2007;48:1162–71. doi:10.2967/jnumed.107.039859.
21. Wu Y, Zhang X, Xiong Z, Cheng Z, Fisher DR, Liu S, et al. microPET imaging of glioma integrin αvβ3 expression using 64Cu-labeled tetrameric RGD peptide. J Nucl Med 2005;46:1707–18.

22. Li ZB, Wu Z, Chen K, Ryu EK, Chen X. 18F-Labeled BBN-RGD heterodimer for prostate cancer imaging. J Nucl Med 2008;49:453–61. doi:10.2967/jnumed.107.048009.
23. Wu Y, Cai W, Chen X. Near-infrared fluorescence imaging of tumor integrin αvβ3 expression with Cy7-labeled RGD multimers. Mol Imaging Biol 2006;8:226–36. doi:10.1007/s11307-006-0041-8.
24. Liu Z, Yan Y, Chin FT, Wang F, Chen X. Dual integrin and gastrin-releasing peptide receptor targeted tumor imaging using 18F-labeled PEGylated RGD-bombesin heterodimer 18F-FB-PEG3-Glu-RGD-BBN. J Med Chem 2009;52:425–32. doi:10.1021/jm801285t.
25. Fani M, Andre JP, Maecke HR. 68Ga-PET: a powerful generator-based alternative to cyclotron-based PET radiopharmaceuticals. Contrast Media Mol Imaging 2008;3:67–77. doi:10.1002/cmmi.232.
26. Lacroix M. MDA-MB-435 cells are from melanoma, not from breast cancer. Cancer Chemother Pharmacol 2009;63:567. doi:10.1007/s00280-008-0776-9.
27. Rae JM, Creighton CJ, Meck JM, Haddad BR, Johnson MD. MDA-MB-435 cells are derived from M14 melanoma cells – a loss for breast cancer, but a boon for melanoma research. Breast Cancer Res Treat 2007;104:13–9. doi:10.1007/s10549-006-9392-8.
28. Cai W, Zhang X, Wu Y, Chen X. A thiol-reactive 18F-labeling agent, N-[2-(4–18F-fluorobenzamido) ethyl]maleimide, and synthesis of RGD peptide-based tracer for PET imaging of αvβ3 integrin expression. J Nucl Med 2006;47:1172–80.
29. Zhang X, Xiong Z, Wu Y, Cai W, Tseng JR, Gambhir SS, et al. Quantitative PET imaging of tumor integrin alphavbeta3 expression with 18F-FRGD2. J Nucl Med 2006;47:113–21.
30. Cai W, Wu Y, Chen K, Cao Q, Tice DA, Chen X. In vitro and in vivo characterization of 64Cu-labeled Abegrin, a humanized monoclonal antibody against integrin αvβ3. Cancer Res 2006;66:9673–81. doi:10.1158/0008-5472.CAN-06-1480.
31. Zhang X, Cai W, Cao F, Schreibmann E, Wu Y, Wu JC, et al. 18F-labeled bombesin analogs for targeting GRP receptor-expressing prostate cancer. J Nucl Med 2006;47:492–501.
32. Chen X, Park R, Hou Y, Tohme M, Shahinian AH, Bading JR, et al. microPET and autoradiographic imaging of GRP receptor expression with 64Cu-DOTA-[Lys3]bombesin in human prostate adenocarcinoma xenografts. J Nucl Med 2004;45:1390–7.
33. Al-Nahhas A, Win Z, Szyszko T, Singh A, Khan S, Rubello D. What can gallium-68 PET add to receptor and molecular imaging? Eur J Nucl Med Mol Imaging 2007;34:1897–901. doi:10.1007/s00259-007-0568-1.